Early human impact in a 15,000-year high-resolution hyperspectral imaging record of paleoproduction and anoxia from a varved lake in Switzerland.

Stamatina Makri[a], Fabian Rey[b, 1], Erika Gobet[b], Adrian Gilli[c], Willy Tinner[b], Martin Grosjean[a]

a. Institute of Geography & Oeschger Centre for Climate Change Research, University of Bern, Erlachstrasse 9a, 3012 Bern, Switzerland
b. Institute of Plant Sciences & Oeschger Centre for Climate Change Research, University of Bern, Altenbergrain 21, 3013 Bern, Switzerland
c. Geological Institute, ETH Zurich, Sonneggstrasse 5, 8092 Zurich, Switzerland
1. Geoecology, Department of Environmental Sciences, University of Basel, Klingelbergstrasse 27, 4056 Basel, Switzerland

Corresponding author

Stamatina Makri

Institute of Geography & Oeschger Centre for Climate Change Research

University of Bern

Erlachstrasse 9a, CH-3012 Bern, Switzerland

E-mail: stamatina.makri@giub.unibe.ch (ORCID iD: 0000-0003-0309-3620)

Co-authors

Dr. Fabian Rey: fabian.rey@unibas.ch (ORCID iD: 0000-0002-0737-3921)

Dr. Erika Gobet: erika.gobet@ips.unibe.ch (ORCID iD: 0000-0002-3487-8108)

Dr. Adrian Gilli: adrian.gilli@erdw.ethz.ch (ORCID iD: 0000-0003-4193-2157)

Prof. Dr. Willy Tinner: willy.tinner@ips.unibe.ch (ORCID iD: 0000-0001-7352-0144)

Prof. Dr. Martin Grosjean: martin.grosjean@oeschger.unibe.ch (ORCID iD: 0000-0002-3553-8842)

Abstract

20th century eutrophication and global spread of anoxia is a threat for freshwater ecosystems. Little is known about Holocene anoxia and meromixis events when anthropogenic impacts were weaker and natural ecosystem variability played the dominant role. In this study, we examine the relationship between lake mixing and lake production, climate variability, vegetation cover, catchment erosion and (pre)historic anthropogenic impacts in Moossee (Switzerland), over the last 15,000 years. We use sub-annually resolved calibrated hyperspectral imaging data (total chlorophyll for paleoproduction, bacteriopheophytin for anoxia and meromixis) combined with X-ray fluorescence and pollen data. Production shows a first increase at 14,500 cal yr BP, a further increase after 7500 cal BP, relative maxima in the late Bronze, Iron and Middle Ages, and the unprecedented peak in the 20th Century. Until 7500 cal BP, the lake was well mixed with only scarce phases of seasonal to multiannual anoxia. Repeated meromixis events occurred between 7500 and 2500 cal BP when temperatures were high, forests closed, and lake production was already enhanced. After the forests were cleared (2500 cal BP) the lake remained mostly holomictic. Holocene meromixis events were systematically terminated by local deforestation related to Neolithic and Bronze Age lakeshore settlements: charcoal peaked, tree pollen dropped below a threshold of 80%, soil erosion and lake production increased and bacteriopheophytin disappeared. Meromixis re-established after the termination of lakeshore settlements and the onset of afforestation with tree pollen exceeding 80%. These repeated cycles unambiguously document how even early human societies affected the mixing regime and biogeochemical cycling in this lake.

Keywords

Paleolimnology; Late Glacial; Holocene; Western Europe; Lake mixing regime; Lake production; Bacteriopheophytin; Land use

1. Introduction

Recent centuries have seen unprecedented environmental change, with multiple stressors putting freshwater ecosystems at stake (Jenny et al., 2016). Adverse ecosystem responses such as eutrophication, hypoxic/anoxic conditions and altered lake mixing regimes (Butz et al., 2017; Smith and Schindler, 2009) have mainly been attributed to modern human impact (Dearing et al., 2006; Gell et al., 2007). Meromictic lakes that do not mix completely and hypoxia are now reported globally, predominantly where intense anthropogenic nutrient loads have prompted eutrophication, water column stability, and anoxia (Hall and Northcote, 2012; Jenny et al., 2016). Nonetheless, humans have affected terrestrial and lake ecosystems for several thousands of years, with impacts highly variable in space and time (Dubois et al., 2018).

The main processes that can create and sustain meromictic conditions are related to physical and chemical properties of lake water that enhance density differences between the lower layer, or monimolimnion, and the upper layer, or mixolimnion (Boehrer et al., 2017). Wind or undercurrents can create internal waves and propagate kinetic energy through the density stratification, which may finally result in cease of meromixis and onset of holomixis (Imboden and Wüest, 1995). Hence, increased production, temperature, and wind exposure are factors that can influence the onset and cessation of lake meromictic conditions.

On the other hand, primary production can be influenced by erosion, landscape development and land use in the catchment or a combination thereof (Hakala, 2004). Development of soils and vegetation increase the pool of organic matter and subsequent nutrient leaching into the lake (Bajard et al., 2017a; Jenny, 1980). Agricultural and pastoral activities in the catchment can have a great effect on soil's nutrient enrichment through manuring by grazing (Bajard et al., 2017b; Jewell et al., 2007). Increased phosphorous and nitrogen can be transferred into the lake through surface runoff altering the nutrient cycle and increasing aquatic production (Bajard et al., 2018; Pini et al., 2017).

Very little is known about meromixis events on longer time scales, such as the Holocene, in general, and more specifically about their onsets, cessations, and potential causes. The major obstacle is the lack of diagnostic proxies in lake sediments that allow millennial-long records at annual to sub-decadal resolution (Friedrich et al., 2014). Diagnostic meromixis proxies such as lipid biomarkers, bacterial DNA, and pigments indicative of bacterial plates at the chemocline (Friedrich et al., 2014; Naeher et al., 2012; Wirth et al., 2013) are intensive and have typically a centennial sampling resolution for Holocene-long records. These methods can use a sampling resolution of typically 0.5 cm at best that would result in (sub)decadal resolution, depending on the sedimentation rate, and with almost no possibility to extend this resolution for millennial-long records. Sulfur burial rates and X-ray fluorescence (XRF)-inferred redox-sensitive metals (Fe, Mn, Mo, and their ratios) provide high-resolution records and are often used in ocean and lake environments (Friedrich et al., 2014; Naeher et al., 2013; Wirth et al., 2013; Żarczyński et al., 2019). In lakes, their interpretation is challenging (see. e.g., Naeher et al., 2013), principally because some of these elements are also related to lithogenic influx and erosion. Another approach has been proposed by Jenny et al. (2013) who used the onset of annual laminations as a marker of hypoxia over the last 150 years.

Recently, Butz et al. (2015) developed a rapid, non-destructive scanning method using hyperspectral imaging (HSI) data to quantitatively infer bacteriopheophytin (Bphe) and total chloropigments (chlorophylls and diagenetic products) in lake sediments at very high spatial resolution (ca. 40 x 40 μm pixel size). After calibration with HPLC data, HSI-inferred Bphe was used to identify phototrophic anoxygenic bacteria, such as purple sulfur bacteria, living at the chemocline in a meromictic lake (Butz et al., 2017, 2016), and total chloropigments were used as a proxy for aquatic production (Schneider et al., 2018). These proof-of-concept studies were performed on short sediment cores from a currently meromictic lake in NE Poland (Butz et al., 2017) and from a monomictic lake in southern Switzerland (Schneider et al., 2018). These studies revealed that (i) HSI-inferred chloropigments are suitable to trace paleoproduction and

recent eutrophication at very fine (sub-varve scale) resolution, and (ii) in the currently meromictic lake in NE Poland, HSI-inferred meromixis (Bphe) persisted for the past 2000 years and was only interrupted during periods of high lithogenic influx and sediment slumping.

Our study is the first to extend HSI-inferred high-resolution records of aquatic production and meromixis in a lake with varved sediments and currently dimictic, Moossee on the Swiss Plateau, to a full deglacial cycle, the Late Glacial and Holocene (Rey et al., 2019b). Our research was guided by three questions: How did anoxia and paleoproduction develop over the past 15,000 years based on sub-seasonal resolution proxy data? What were the forcing factors with regard to landscape evolution, land use and climate? What was the role of prehistoric and historic anthropogenic human impact? We use calibrated Bphe and total chlorophylls concentrations inferred from hyperspectral indices, as demonstrated by Butz at al. (2015), to reconstruct an annual to sub-annual resolution record of anoxia, meromixis and paleoproduction. We combine this information with XRF data acquired at a similar spatial resolution, and with pollen and charcoal data with resolution of 10–11 years (Rey et al., 2019a, 2019b). We have chosen Moossee for this study because (i) it contains a complete and almost entirely varved sediment record for the Late Glacial and Holocene (Rey et al., 2019a, 2019c); (ii) it was dated using high-precision radiocarbon wiggle-matching (Rey et al., 2019a, 2019c); and (iii) high-resolution pollen and microscopic charcoals records exist (Rey et al., 2019a, 2019b). In addition, the lake and its surroundings have a unique, very well-documented archaeological record (Harb, 2017). These characteristics provide a rare opportunity for a holistic paleoenvironmental reconstruction and insight into coupling between the catchment and the lake at very fine detail.

2. Study site

Moossee (47°1'17.0''N, 7°29'1.7''E; 521 m a.s.l) is a small exorheic lake 8 km from Bern, on the western Swiss Plateau (Fig. 1a). It has a maximum depth of 22 m and a surface area of

104 0.31 km^2 (Fig. 1b) (Guthruf et al., 1999). The lake is currently eutrophic to polytrophic and
105 monomictic/dimictic (see Fig. S1 in supplementary material), with anoxic bottom waters during
106 summer stratification (Guthruf et al., 1999, 2015). Currently, algal biomass in the water column
107 is dominated by bacillariophyceae, chlorophyceae and cryptophyceae; bacteriophyta were not
108 found in 2003 and only in traces in 2013 (Guthruf et al., 2015). The hydrological catchment
109 surface is 20.8 km^2 and today is mostly used for intensive agriculture (Guthruf et al., 1999).
110 Forests are restricted to mixed beech on the surrounding hills and alder and ash directly along
111 the lake shore (Rey et al., 2019a). The climate of the region is temperate with mean annual
112 temperatures of 8.8°C and mean annual precipitation of 1057 mm (Bern/Zollikofen station,
113 MeteoSwiss, 2019).
114

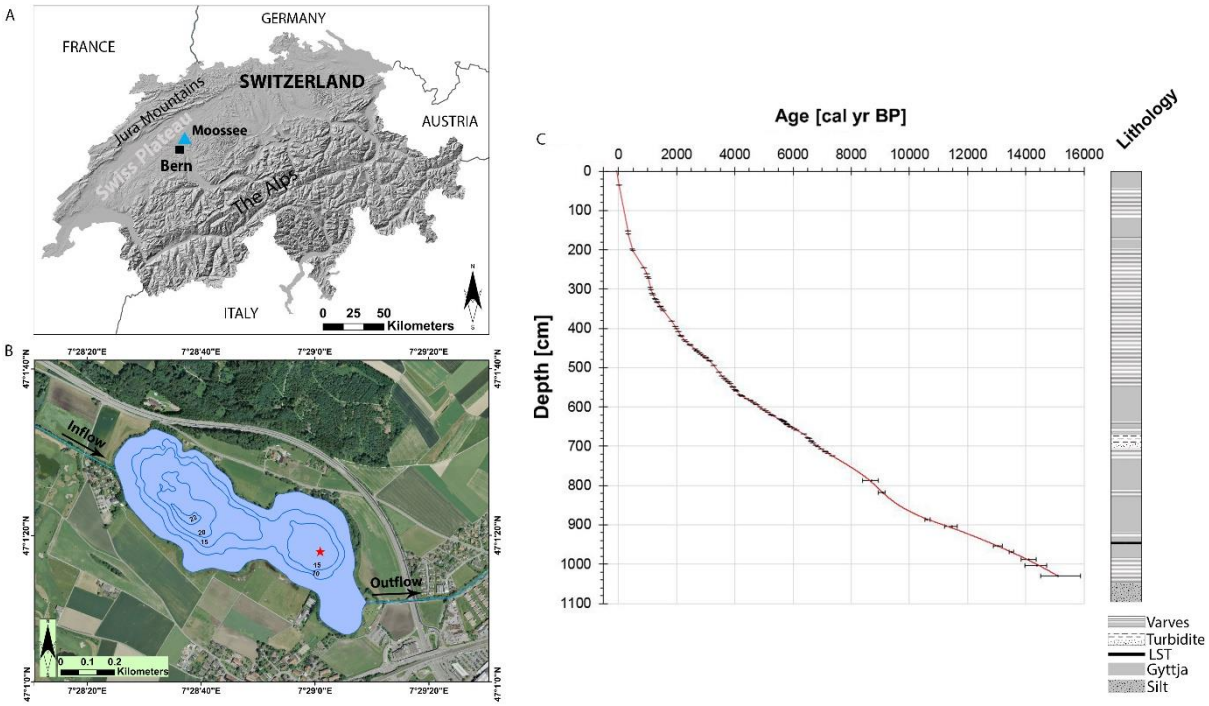

115

116 **Fig 1:** a) Localization of Moossee. b) Bathymetric map of the lake, indicating the coring
117 position with a star. c) Age-depth model and lithology of cores A-C. The topmost 7 m are
118 stratigraphically correlated with the cores F-H of Rey et al. (2019a, 2019b); the chronology
119 between 7 and 10.4 m is identical to the chronology of Rey et al. (2019a). LST marks the
120 Laacher See Tephra.

Moossee was formed during the retreat of the Rhône Glacier around 19,000 years ago (Guthruf et al., 1999). The bedrock is composed of Tertiary molasse carbonaceous sandstone overlain by glacial till (Schmid et al., 2004). After the deglaciation, soil profiles show periglacial cover beds mixed with loess loam and slope wash in the Early Holocene (Veit et al., 2017). After 7.5 ka BP soils indicate landscape stability and surficial mixing by bioturbation (Veit et al., 2017). Histosols rich in organic matter and Gleysols developed around the lake, and Luvisols in the catchment ("Geoportal des Kantons Bern," 2019).

The lowland region of the Swiss Plateau was favorable for early human settlements and agriculture. After the lake level lowering in 1856 CE, several Neolithic and Early Bronze Age lakeshore settlements emerged; these were dated to discrete periods between 6500 and 3600 cal BP (Harb, 2017). During these periods, increased *Cerealia-type*, *Plantago-lanceolata* and *Urtica* (Rey et al., 2019a) indicate forest disruption and land use for arable and pastoral farming. Bern, ca. 8 km south of the lake, has been inhabited since the Iron Age followed by massive forest openings and intensification of agricultural activities, with further increase in cultural indicators and sporadic *Sporormiella* fungal spores suggesting pastoral farming close to the lake (Rey et al., 2019a).

In 2014, Rey at al., (2019a, 2019b, 2019c) retrieved five parallel sediment cores and developed a high-precision chronology (Rey et al., 2019a, 2019c; Fig. S2). A high resolution (10-11 years) record of pollen and microscopic charcoal was established for the section between 7000 and 3500 cal BP and at 250–300 years resolution for the rest of the core (Rey et al., 2019a, 2019b).

3. Material and methods

For this study, we used the sediment cores A-C of ca. 10 m total length. The uppermost 7 m were stratigraphically correlated to the core dated by Rey et al. (2019a) using ca. 100 tie

points (varves and marker layers; see supplementary material Table S1). Ages between the tie points were linearly interpolated. The chronology below 7 m sediment depth is identical to Rey et al. (2019a) (see supplementary material Fig. S2).

XRF core scanning was performed at continuous 1 mm steps using the Avaatech core scanner at ETH Zurich. An area of 1 mm by 12 mm was measured for 20 seconds at 10kV (1500 μA) and at 30 kV (2000 μA). From the detected elements, Ti was used as an indicator of higher lithogenic erosional input from the catchment, and Ca as an indicator of endogenous calcium carbonate precipitation (Koinig et al., 2003). P was associated with anoxic conditions and limited mixing (Boehrer et al., 2017; Hongve, 1997).

Hyperspectral Imaging (HSI) scans were made using the A-C core halves using a Specim PFD-xx-V10E camera, with spectral range 400–1000 nm, slit width 30 μm and spectral resolution 2.8 nm. We used a spatial resolution of ~68 μm per pixel with a spectral sampling of 1.57 nm. After scanning, data was post processed using the ENVI software version 5.4 (Exelis Visual Information Solutions, Boulder, Colorado) following Butz et al. (2015). Spectral endmembers were used to calculate the relative absorption band depths (RABDs) following Butz et al. (2015). The $RABD_{673}$, with maximum absorption at 673 nm (Equation 1), was used to diagnose total chlorophylls (TChl), that is, chlorophylls (mainly *a* and b) and their degradation products, to be used as a proxy for aquatic primary production (Leavitt and Hodgson, 2001). However, taxa with high chl c content are not taken into account as they have weak absorption in this range. The $RABD_{845,}$ with maximum absorption at R_{845} nm (Equation 2) was used as a diagnostic for bacteriopheophytin (Bphe: sum of Bphe *a* and *b*) following Butz et al. (2016, 2015). Bphe is a degradation product of Bacteriochlorophyll, produced by anoxygenic phototrophic bacteria, such as purple sulfur bacteria, in the chemocline of meromictic lakes where light is available (Yurkov and Beatty, 1998).

$$\text{RABD673 nm} = \left(\frac{59 * R584\,nm + 88 * R730.7\,nm}{147}\right) / R671.9\,nm \quad (Eq.\,1)$$

$$\text{RABD845 nm} = \left(\frac{55 * R791.4\,nm + 55 * R900.3\,nm}{110}\right) / R845.9\,nm \quad (Eq.\,2)$$

The spectral indices $RABD_{673}$ and $RABD_{845}$ were calibrated with absolute pigment concentrations of extracts from selected sediment samples measured by spectrophotometry (Shimadzu UV-1800). For this proxy–proxy calibration, 44 sediment samples (1 cm slices) were taken from specific sites in the sediment sequence, following Butz at al.'s (2015) methodology. Sampling was optimized for the calibration of $RABD_{673}$ values so that a wide range of RABD values was covered and the values were evenly distributed along the gradient. Each sample consisted of several varves. Parts of the sediment core with very high RABD values and high varve-to-varve variability were avoided to increase the calibration quality (Butz et al., 2017). Pigments were extracted with an adapted version of Schneider at al.'s (2018) method, using pure acetone, supernatant evaporation under nitrogen, and dilution with 2 ml of pure acetone. We verified the spectrophotometric analysis with analytical standards from Sigma-Aldrich and DHI. We calculated the absolute pigment concentrations using the molar extinction coefficient for Bphe *a* by Fiedor et al. (2002), and the molar extinction coefficient for chlorophylls and chlorophyll derivatives adapted by Jeffrey et al. (1975).

RABD values were calibrated to photospectrometrically measured TChl and Bphe concentrations with linear regression models following Butz et al. (2015). The quality of our regression model was assessed using R^2 and R^2_{adj} adjusted for the degrees of freedom, and the root mean square error of prediction (RMSEP) was assessed using the 10-fold, leave-one-out (k-fold) and bootstrap methods in R (R Core Team, 2015) (see Fig. S3 in supplementary material). The calibration model for TChl (Fig. S3a) shows a Pearson correlation r = 0.93 and a coefficient of determination R^2 = 0.8727 (R^2_{adj} = 0.8697, $p < 0.001$), with an average

uncertainty of ~ 9% (ca. 190 μg g^{-1} dry mass). For $RABD_{673}$ values smaller than 1.058, our calibration model calculates negative concentrations. This offset is attributed to a matrix effect in the hyperspectral data where the continuum between the endpoints of the trough (Equation 1) is not a linear slope. The calibration model for Bphe shows a $r = 0.96$ ($p < 0.001$), with a coefficient of determination $R^2 = 0.9189$ ($R^2_{adj} = 0.9134$) (Fig. S3b). The Shapiro-Wilk and the Kolmogorov-Smirnov tests of the residuals show they are most likely normally distributed, thus inference is valid using these models. Accordingly, our calibration model for TChl is valid for the rage between ca. 190 and 2200 μg g^{-1} dry mass and for Bphe in the range between ca. 4 and 38 μg g^{-1} dry mass.

Statistical analysis was performed in R using the add-on packages RIOJA for clustering and VEGAN for PCA (R Core Team, 2015). To investigate the relationships between variables defining different sediment facies (TChl and Bphe concentrations, Ti, P and Ca), we performed an unconstrained hierarchical clustering using the Euclidean distance matrix and the ward.D2 clustering method in R (Murtagh and Legendre, 2014). A 10-year smoothing filter was applied to the resulting clusters. To track the major changes in the mixing regime and catchment parameters, we performed a PCA analysis on the full multi-proxy dataset, including pollen sums (tree pollen [TP], herbs, shrubs, cultural indicators), and microscopic charcoal influx (particles cm^{-2} yr^{-1}, Rey et al., 2019a), and chironomid-inferred summer temperature (Heiri et al., 2015). TP was used to detect undisturbed, rather closed forest cover that might fence against wind and act against erosion. The cultural indicators pollen sum consists of Cerealia (*Hordeum*-type, *Triticum*-type, *Avena*-type, *Secale cereale*), *Plantago lanceolata* and *Linum usitatissimum*. This multiproxy dataset also underwent constrained hierarchical clustering using the Bray distance and ward.D2 linkage method in R. The broken stick model was used to determine the significant groups in the cluster analysis and to assess the likely statistical significance of the axes in the PCA. Data were log transformed to stabilize their variance and then standardized prior to statistical analyses.

4. Results

4.1 Seasonal (sub-varve) to interannual variability of Bphe and TChl concentrations.

Fig. 2 shows close-ups of sediment varves including the time series of $RABD_{845}$ and $RABD_{673}$ values and calibrated concentrations for Bphe and TChl, respectively. In the color infrared images, light laminae represent spring and early summer layers of calcite deposition. The lower part of the dark laminae represents late summer to fall deposition, whereas their upper part represents winter organic and inorganic detritus deposition. The 68 μm spatial resolution of the RABD index values allows us to observe seasonal patterns of pigment deposition within individual varve years. Varves are typically around 0.5-1 mm in thickness.

Fig. 2a,b shows a close-up of three varve years in 4-mm core segment at 690 cm core depth, ca. 6670 cal BP. It comes from a segment where Bphe is present but at very low concentrations. The distribution pattern of Bphe concentrations is generally the same for all three varve years, with overall higher values during summer in the light layers and lower values during winter in the dark layers. The negative anomalies observed in the white layers are due to dilution caused by rapid calcite precipitation. However, lower values are also observed when TChl concentrations peak. The distribution pattern of TChl concentrations (Fig. 2b) shows differences from year to year. Within the lower two varve years (6904-6901 mm), one green algae bloom with higher TChl concentrations during early summer (light layers) and lower concentrations during fall/winter (dark layers) can be observed. In the third varve year (6901-6900 mm), two algal blooms, one in spring and another one in the second half of the year (fall) is found. Overall, TChl values in the white layers may appear lower due to higher precipitation of calcite during summer (dilution effect).

Fig. 2c,d shows a close-up of four varve years in a 1.6-mm long segment at 622 cm core depth, around 5310 cal BP. It comes from a meromictic period with high Bphe concentrations (Fig. 2c). Here, the distribution of Bphe shows persistently high concentrations throughout the

seasons (dark and light layers). TChl concentrations (Fig. 2d) are overall higher in the light layers and lower in the dark layers. Two additional varve close-ups, one in the Allerød and another one in the Middle-Ages (Fig. S4 and S5 in supplementary material) are discussed in Section 5.2.

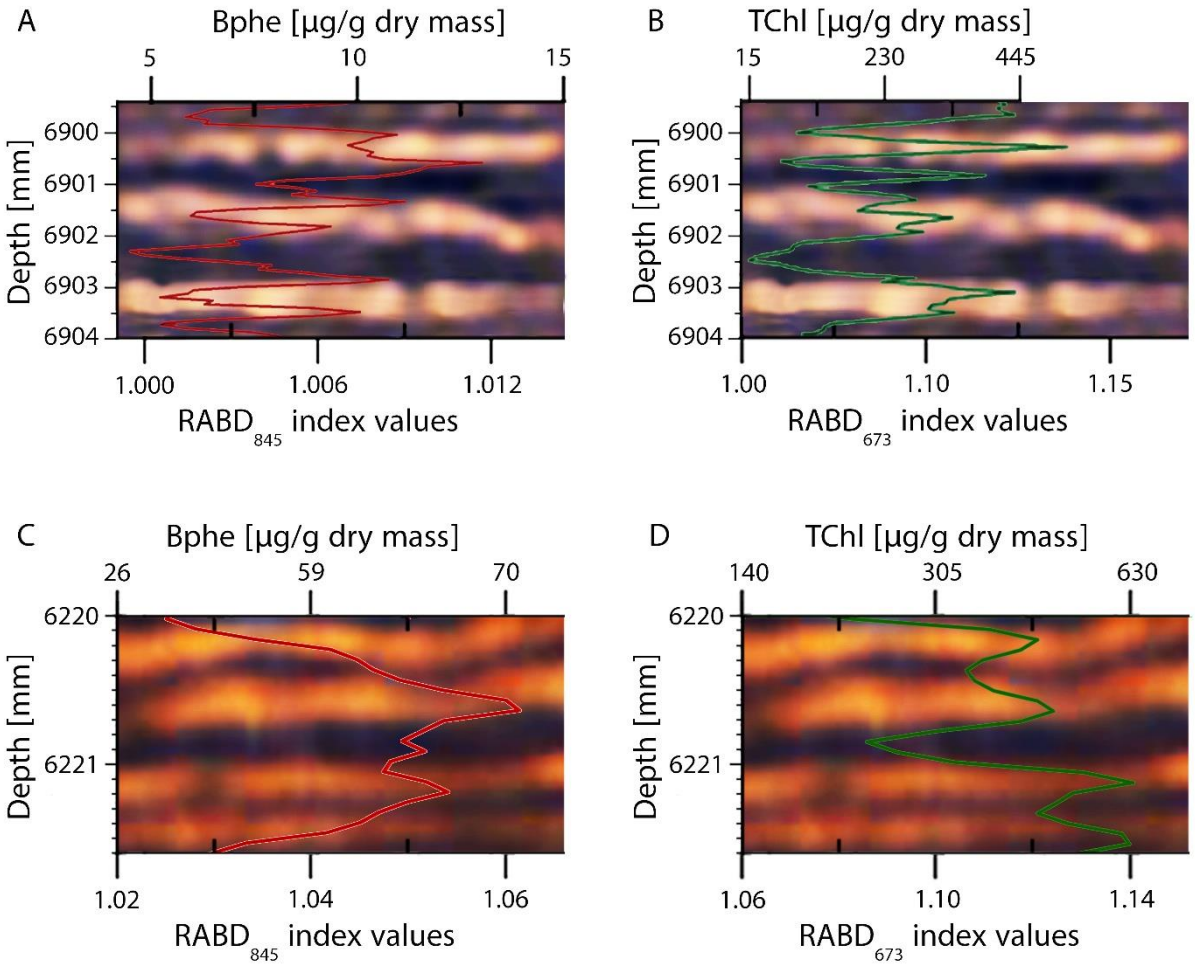

Fig. 2: Color infrared (CIR) close-up images showing the distribution of Bphe (left, in red) and TChl (right, in green) concentrations within individual varves. In a,b) the three varve years are from a sediment section at 690 cm core depth (ca. 6670 cal BP) with generally low Bphe concentrations and mostly seasonal anoxia. In c,d) the four varve years (1.6-mm long section at 622 cm sediment depth, ca. 5310 cal BP) show persistently high Bphe concentrations suggesting meromixis.

4.2 Sedimentology and biogeochemical proxies

The sediment lithology and time series of the biogeochemical proxies are presented in Fig. 3. The sediments are almost entirely laminated, interrupted by a few intervals of homogenous sediment deposition with diffuse laminations. Around 13,034 cal BP, the core exhibits a distinctive bluish gray (GLEY 2 5/1) 1 cm thick layer of the Laacher See Tephra (LST). Regular sediment deposition is interrupted by a large turbidite of 20 cm around 9700 cal BP. Otherwise the sedimentation is continuous. According to the age-depth model (Fig. 1c), the sedimentation rate is relatively constant from 15,000 to 2000 cal BP with values between 0.05 to 0.1 cm y^{-1}. After 2000 cal BP, the sedimentation rate increases ranging mainly between 0.2 to 0.5 cm y^{-1} in response to higher erosional input and primary production.

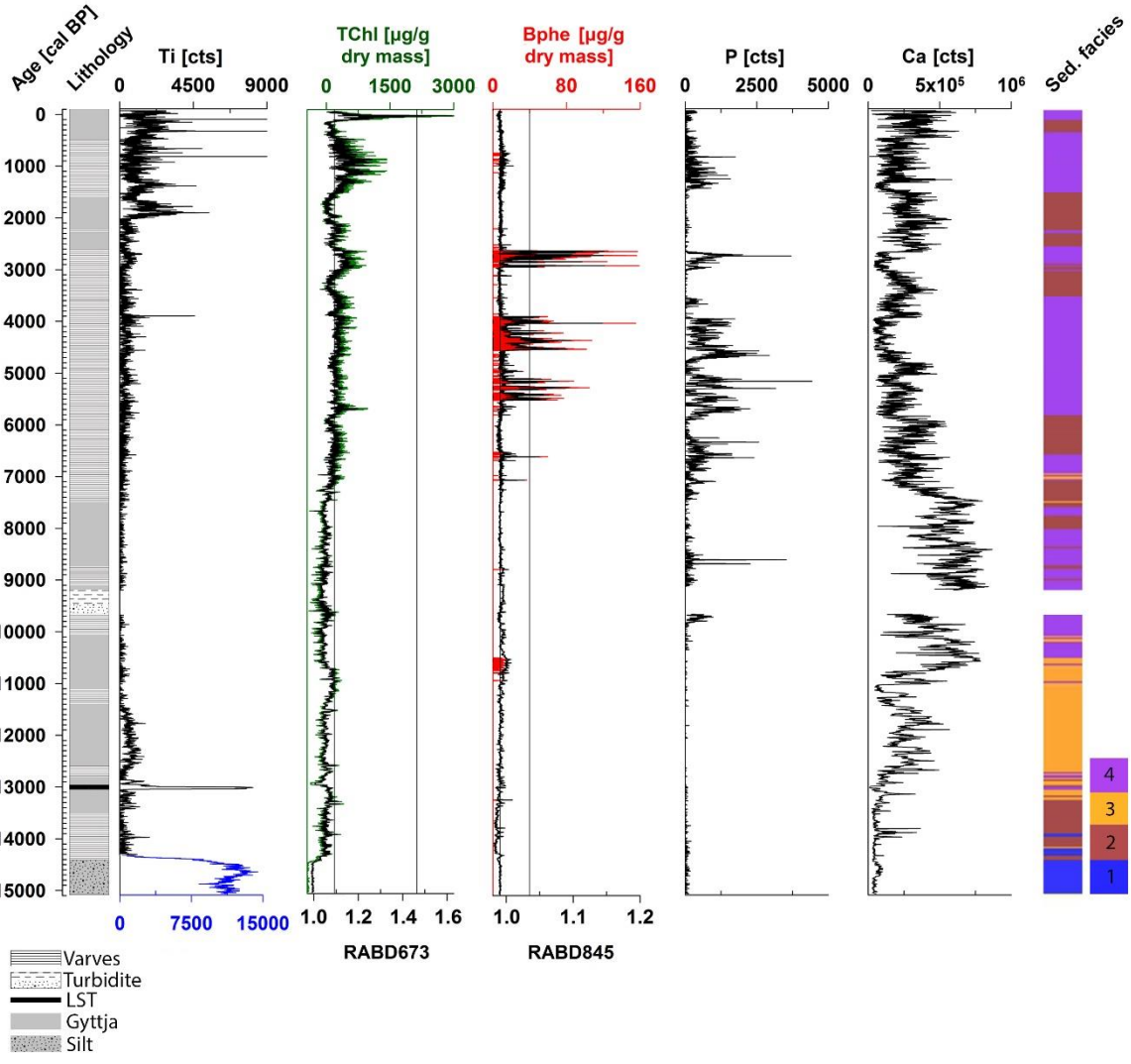

Fig. 3: Sediment description and biogeochemical proxies (selected XRF data and hyperspectral indices) of Moossee. For Ti, the blue color at the bottom refers to the separate scale. In the TChl and Bphe time series, black color shows the RABD index values and green and red colors indicate TChl and Bphe concentrations, respectively. The vertical black lines represent the lower and upper limits of the calibration models. The multicolor column on the right indicates the sediment facies defined by unconstrained clustering (see text)

Ti counts, indicative of erosional input to the lake, are very high from ca. 15,076 to 14,400 cal BP (Fig. 3). At ca. 14,400 cal BP, Ti decreases sharply, indicating a transition to lower erosion and landscape stability. At 13,034 cal BP (± 150 years) our record shows the characteristic peak of the LST dated to 12,934 ± 165 cal yrs BP (Baales et al., 2002). From 12,800 to 11,700 cal BP, the Younger Dryas, Ti counts increase, suggesting enhanced geomorphological surface processes. After this period, Ti counts remain at low levels until 7500 cal BP. From 7500 to 2000 cal BP, lithogenic indicators increase weakly and gradually with a local maximum at around 3900 cal BP, the beginning of the Bronze Age. Around 2000 cal BP, the Roman Period, Ti counts increase significantly and stay high until recent times. Ti counts show a distinct maximum around 800 cal BP (the Middle Ages), 300 cal BP (the Little Ice Age) and 100 cal BP (the 19th century Industrial Period).

Calibrated TChl concentration is indicative of aquatic primary production. From ca. 15,100 to 14,400 cal BP, TChl remains at minimal levels (Fig. 3). At 14,400 cal BP, TChl increases, yet remains overall at relatively low levels until 7500 cal BP. Around 7500 cal BP, production further increases significantly with distinct peaks from 5700 to 5600 cal BP (Neolithic), from 3000 to 2600 cal BP (Late Bronze and Iron Age), and from 1300 to 700 cal BP (Middle Ages). From 550 to 150 cal BP (Little Ice Age), TChl decreases substantially. Finally, from 90 cal BP onward, in the mid-19th century, TChl values reach their highest levels overall.

Bphe concentrations indicate seasonal anoxia and meromictic conditions in the lake. From ca. 15,100 to 7500 cal BP, Bphe remains mainly absent (Fig. 3), suggesting that holomictic conditions prevailed. In this period, there is one instance where Bphe was detected (from 10,850 to 10,500 cal BP) with low concentrations over a longer period. Two other possible episodic anoxia events (Allerød interstadial around 13,350 cal BP and at around 8800 cal BP) are close to the detection limit and unclear. After 7500 cal BP, periods with detectable persistent Bphe concentrations appear more frequently, suggesting short-term meromictic events around 7000 cal BP, 6600 cal BP, and 5700 cal BP, each lasting from 50 to 150 years. Persistent periods with abundant Bphe occur in the Mid-Holocene, in 5500–5050 cal BP, 4550–3900 cal BP, and 3000–2600 cal BP. From 2600 cal BP onward, Bphe is mainly absent, except for a small increase between 700 and 1000 cal BP (Middle Ages), yet with low concentration close to the detection limit. Generally, P counts follow lake production (TChl) and anoxia events (Bphe) closely. P is hardly detectable before 7500 cal BP but increases overall thereafter. During periods with high Bphe values, P counts reach relative maxima.

Ca counts, here indicating endogenous calcium carbonate concentrations, are low from ca. 15,100 to 12,800 cal BP (Fig. 3). From 12,800 to 11,700 cal BP (Younger Dryas), Ca shows an increase with some fluctuations. Highest values are found between 10,700 and 7500 cal BP, whereas from 7500 to 2600 cal BP, Ca values decrease overall. Minimum Ca values around 5100 cal BP, 4550–3900 cal BP, and 3000–2600 cal BP coincide with maxima in Bphe. From 2600 cal BP onward, Ca counts increase again.

Unconstrained clustering of selected geochemical proxies (Ti, TChl, Bphe, P and Ca) resulted in four sedimentary facies (Fig. 3) described as follows:

Facies 1 is only found at the bottom of the core from 15,087 to 14,400 cal BP. It consists of light gray (7.5YR 7/1) homogenous silt and is characterized by low production (TChl), low calcium carbonate content (Ca), and high lithogenic erosional input (Ti), suggesting unstable landscape conditions.

Facies 2 is found in several parts of the core sequence. The sediment color varies from dark grayish brown (7.5YR 4/2) clay with very pale brown (7.5YR 8/2) calcareous varves, to gray (2.5Y 5/1) clay with diffuse light (2.5Y 7/1) and dark gray (2.5Y 4/1) laminations. It is mainly characterized by moderate production and calcium carbonate contents, as indicated by the presence of TChl and Ca, respectively.

Facies 3 occurs from ca. 13,250-10,500 cal BP and consists of light brownish gray (2.5Y 6/2) clay, with some occasional very thin light gray (2.5Y 7/2) and gray (2.5Y 5/1) silty beds, as well as dark grayish brown (2.5Y 3/2) varves, with very pale brown (10YR 8/2) calcareous varves in some parts. TChl concentration is low, and calcium carbonate content (Ca) is high.

Facies 4 occurs in several parts of the core sequence and alternates with Facies 2. In Facies 4, we find very dark gray (2.5Y 3/1) clay with light gray (10YR 7/1) calcareous varves and some gray (2.5Y 5/1) clay with dark grayish brown (10YR 4/2) and light gray (10YR 7/2) diffuse laminations. Facies 4 is characterized by high production (TChl) and anoxic conditions with limited mixing (high Bphe, P).

5. Discussion

5.1 Mixing regime changes inferred from seasonal distributions of Bphe and TChl in varves.

The calibration of the $RABD_{673}$ and $RABD_{845}$ versus TChl and Bphe spectrophotometer-inferred concentrations shows robust calibration statistics (Fig. S3 supplementary material) with an uncertainty of ~10%, which is comparable with previous studies of paleoproduction reconstructions over short time scales (Butz et al., 2017, 2015; Das et al., 2005; Schneider et al., 2018). The high spatial resolution of ca. 68 μm on sample pixel size of HSI data combined with robust calibration models of spectral indices provide unprecedented insight into seasonal structures of pigment concentrations in varved sediment (Fig. 2). This permits to assess the phenology of algal blooms throughout the year, and to assess whether anoxia was a seasonal or

a perennial phenomenon. The calibration model has limits for low values: for Bphe is 8 μg/g dry mass with average RMSEP of 3.26 μg/g dry mass and for TChl 190 μg/g dry mass (average RMSEP).

The distribution of Bphe within individual varves in periods of low concentrations (Fig. 2a) follows a seasonal annual cycle with higher values during summer and lower values during winter, rather than persistently high values throughout the years. In this case, phototrophic bacteria develop in the upper part of the anaerobic and sulfide-containing hypolimnion during summer stratification (Imhoff, 2014). Similar observations have been made in several other seasonally stratified lakes (Diao et al., 2017; Vila et al., 1998). Contrarily, in periods of high Bphe concentrations (Fig. 2c) the distribution within the varves indicates the presence of a persistent bacterial plate throughout all seasons suggesting the establishment of meromictic conditions in the lake (Tonolla et al., 2003).

The distribution of TChl in both cases (Fig. 2b,d) follows normal seasonal changes, with generally higher values during spring and early summer and lower ones during late summer and winter except for years with a second algal bloom in autumn (Fig. 2b at 6899.5 mm). The μm scale of the HSI technique enables us to differentiate years with one bloom of chlorophyll-bearing algae in spring from those with two, one in spring and the other in fall. This type of information bears a great potential for paleoclimatic interpretations, which still needs to be explored. Interestingly, during phases of TChl peaks in early summer (Fig. 2b, light layers), Bphe values are relatively low. This could be attributed to a dilution effect arising from high carbonate precipitation and TChl and, to some extent, to light competition in the epilimnion. In spring, green algal blooms in the epilimnion decrease transparency, creating poor light conditions at the thermocline or the chemocline. In late summer, nutrients are depleted in the epilimnion, and transparency increases, providing higher light intensity in the sulfide-containing layers, hence better conditions for the anoxygenic phototrophic bacteria to develop (Meyer et al., 2011; Parkin and Brock, 1980; Tonolla et al., 2005). This effect is better observed

in the case of seasonal stratification (Fig. 2a,b) where TChl are very high and Bphe concentrations are low.

5.2 Late Glacial /Holocene lake-landscape evolution

We examined the potential relationships between aquatic production, mixing regime, vegetation structure and composition, land use, and summer temperatures by running a PCA analysis (Fig. 4) on the multiproxy dataset. This consists of the $RABD_{673}$, $RABD_{845}$, Ti, P, Ca XRF counts, trees, shrubs, herbs and cultural indicators pollen sums (Rey et al., 2019a, 2019b), and chironomid-inferred summer temperature from the Alpine region (Heiri et al., 2015). The PCA biplot shows that anoxia ($RABD_{845}$) is highly correlated with aquatic primary production ($RABD_{673}$) and P. Aquatic production and anoxia seem to be less dependent on summer temperature and, together with tree pollen, are positively correlated with PC1 as proxies for lake production and forest dominance (Fig. 4). Erosional input inferred from Ti together with herbs, cultural indicators, and charcoal are positively correlated with PC2, which represents land use and fire activity (Fig. 4), and disturbance in general. Interestingly, proxies of biotic drivers such as forest cover, open land, and land use predominate over non-biotic effects such as erosion in driving overall lake evolution and aquatic and terrestrial ecosystem change.

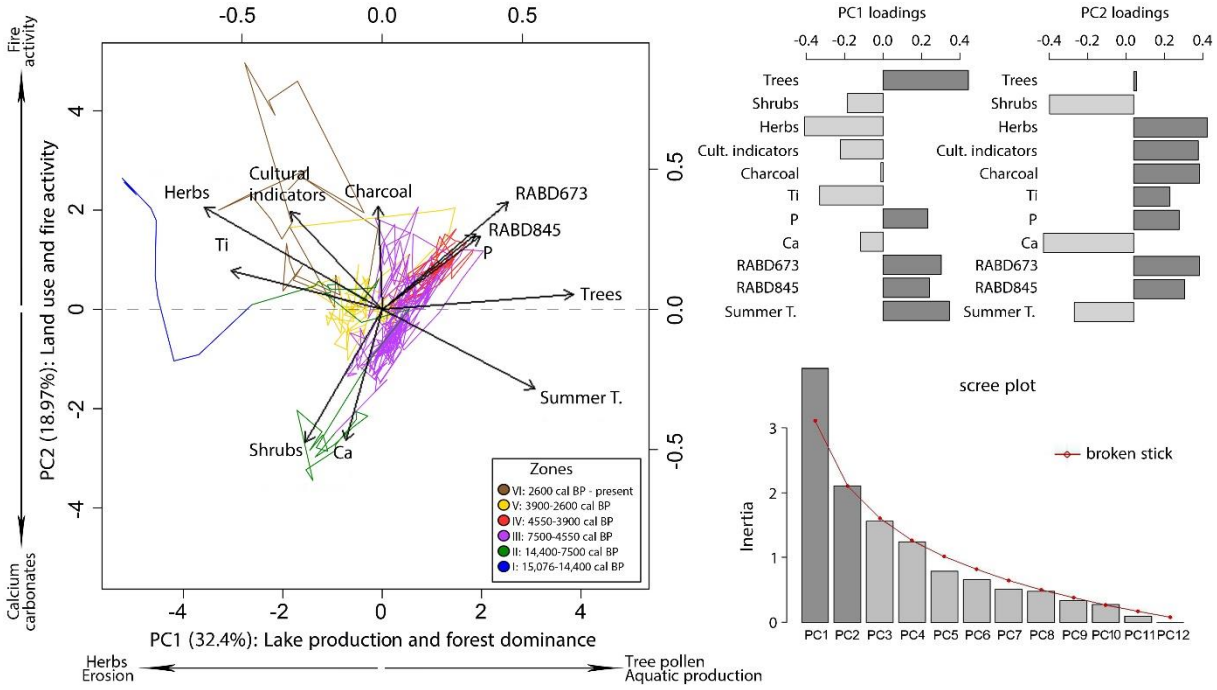

Fig. 4: PCA biplot of the multi-proxy dataset for the first two significant components PC1 (lake production and forest dominance) and PC2 (land use and fire activity), as indicated by the broken stick model (on the bottom right). The different line colors represent the various zones of lake evolution, as defined by constrained clustering, drawing temporal trajectories.

Constrained clustering on the multi-proxy dataset reveals six zones that run trajectories in the PCA ordination space, influenced by different variables through time (Fig. 4 and 5). These six temporal phases that are discussed below summarize the main interactions between the lake biogeochemical state, land use, and climate. Fig. 6 outlines these phases in a conceptual illustration.

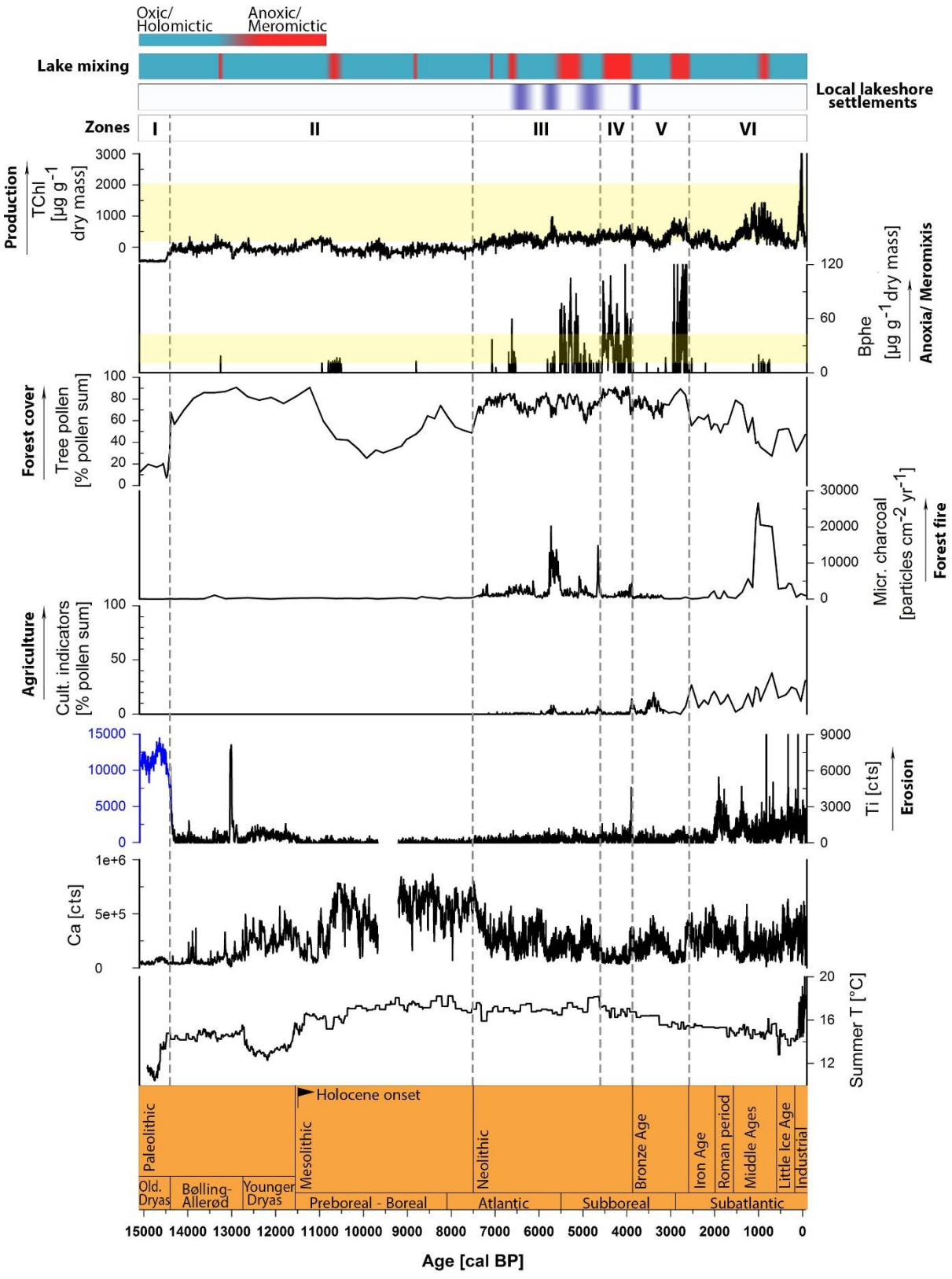

407

408 **Fig. 5:** Synthesis of the multi-proxy dataset including tree pollen, microscopic charcoal, cultural

409 indicators (Rey et al., 2019a), and chironomid July temperatures from the Alpine region (Heiri

410 et al., 2015). Top: the lake mixing regimes and archaeological evidence of human settlements

(Harb, 2017). Bottom: the archaeological epochs and Holocene chronozones (Blant et al., 2010; Lang, 1994, and citations in the text). The blue color in the Ti profile refers to the blue scale on the left separating a period of very high Ti counts (late Oldest Dryas). Vertical dashed lines indicate the lake evolution zones defined by constrained clustering.

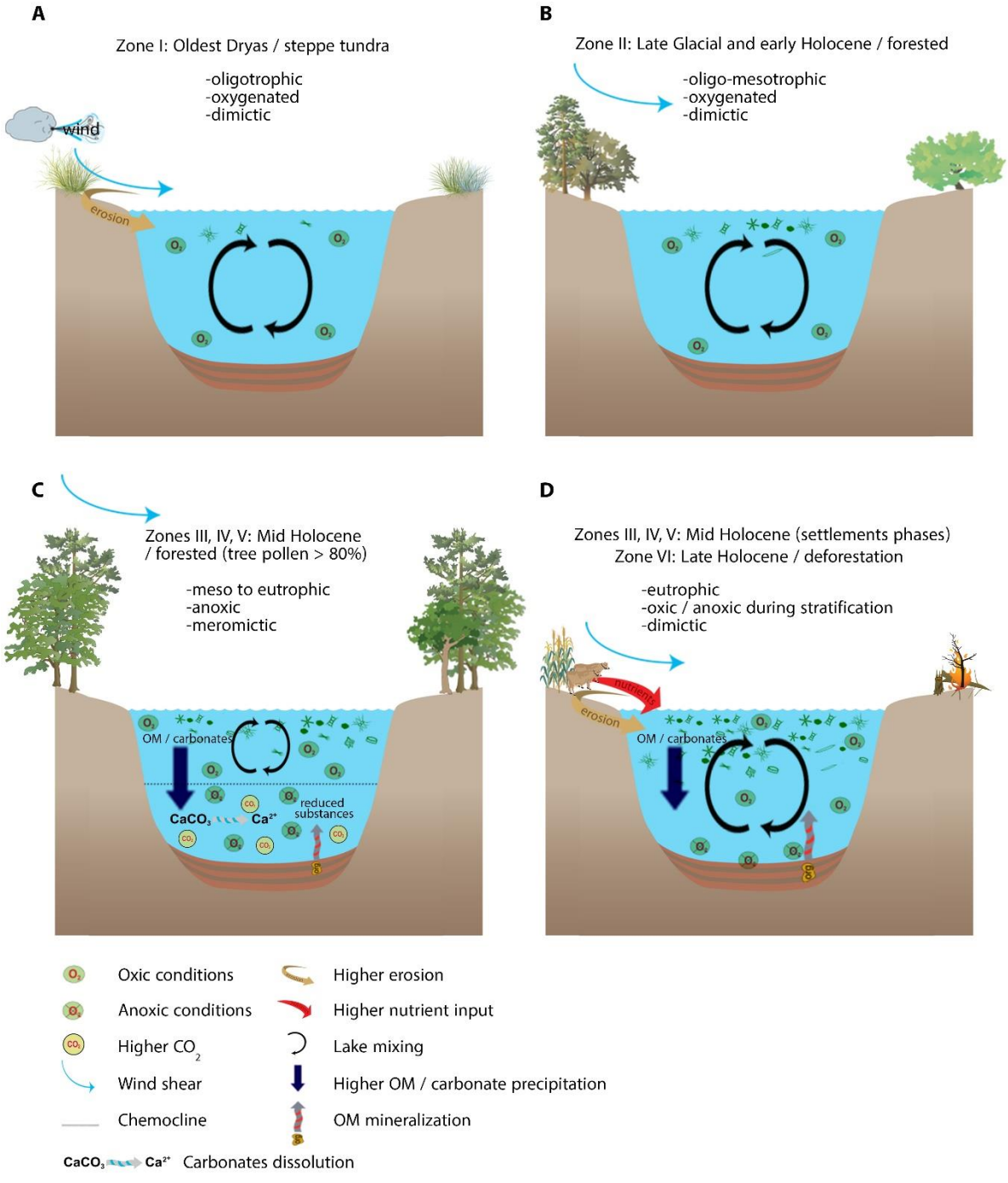

Fig. 6: Conceptual illustration of the main lake-catchment interactions and lake biogeochemistry changes with respect to landscape evolution and human impact for the last 15,000 years (Section 5.2). The different zones were defined after constrained clustering on the multi-proxy dataset shown in Fig. 5.

5.2.1 Zone I (ca. 15,076–14,400 cal BP)

Zone I corresponds chronologically to the late Oldest Dryas (Rey et al., 2017). Sediments are mostly clastic with low aquatic production and carbonate contents. Bphe is absent. The lake was oligotrophic, holomictic, and well-oxygenated, and summer temperatures were still too cold (Heiri et al., 2015) to initiate extensive endogenic carbonate precipitation (Fig. 5, 6a). Substantial clastic sediment formation is expected in an unstable landscape with grass steppe vegetation (Ammann, 1985) and a soil surface highly susceptible to erosion. The first tree birch stands established around 16,000 cal BP (Rey et al., 2017), possibly in response to warmer conditions (Samartin et al., 2012), but steppic tundra prevailed. Similar observations are reported from other Swiss and Central European lakes (Niessen and Kelts, 1989; Schmidt et al., 2002).

5.2.2 Zone II (14,400–7500 cal BP)

During the period 14,400–12,800 cal BP, which roughly corresponds to the Bølling/Allerød interstadial (14,700–12,650 cal BP) (Ammann et al., 2013b, 2013a; Lotter et al., 2012), sediments are finer with some varved parts. Lake production and carbonate content increase slightly (Fig. 5). Erosional input decreased due to the further expansion of boreal birch- and pine-dominated forests (Rey et al., 2017) and the resulting soil stabilization (Ammann et al., 2013b). The relative increase in production and calcium carbonate precipitation in the Allerød agrees with the warmer summers (Fig. 5). Traces of Bphe appear in the Allerød around 13,250 cal BP. A closer examination of laminated sediments in that part (see Fig. S4 supplementary

443 material) shows seasonal anoxia likely due to stronger thermal stratification. Stronger summer
444 stratification was also favored by the concurrent establishment of pine forest with tall trees in
445 the catchment, which reduced wind exposure. All these factors, together, may have contributed
446 to short-term episodic bottom-water anoxia and development of weak bacterial plates at the
447 thermocline (Diao et al., 2017). Similar observations in the same period have been made in
448 Längsee in Austria, with establishment of meromictic conditions slightly before the LST layer
449 (Schmidt et al., 2002), and in Soppensee and Lobsigensee on the Swiss Plateau (Löffler, 1987;
450 Lotter, 2001). These observations agree with studies that have shown that both reduced ice
451 cover duration and significant surface water warming can lead to prolonged stratification and/or
452 anoxia (Schmidt et al., 2002; Woolway and Merchant, 2019).

453 From 12,800 to 11,700 cal BP (Younger Dryas 12,650-11,700 cal BP; Rach et al., 2014),
454 sediments become more homogeneous with occasional coarser sediment beds; TChl remains
455 unchanged, whereas carbonates and erosion increase. Palynological reconstructions report
456 continuously forested landscapes since the Bølling, yet with forest thinning during the YD
457 cooling (Lotter, 2001; Rey et al., 2017; Tinner et al., 2005). Increased lithogenic input to the
458 sediments is also consistent with periglacial activity found in catenas on the Swiss Plateau by
459 Mailänder and Veit (2001). Bphe is absent. Thus, the lake was still oligotrophic and well mixed
460 (Fig. 6b).

461 After the onset of the Holocene, from ca. 11,700 to 7500 cal BP, sediments consist mostly
462 of muddy clay partly varved with higher carbonate contents resulting from higher summer
463 temperatures (Heiri et al., 2015). The YD/Holocene transition is characterized by an increase
464 in lake production, peaking around 11,000 cal BP, which is seen as a response to the rapid
465 postglacial warming (Fig. 5). Between 10,500 and 7500 cal BP, production decreases slightly.
466 Our findings are also confirmed at other sites on the Swiss Plateau, such as Lake Neuchâtel
467 (Schwalb et al., 1998) and Soppensee (Lotter, 2001). As expected, erosion decreases after the
468 mass expansion of temperate trees and shrubs (e.g. *Ulmus, Quercus, Tilia, Corylus avellana*)

(Rey et al., 2017). Bphe is mostly absent. Aquatic production was likely still too low to induce widespread prolonged anoxia during this time.

5.2.3 Zones III, IV, V (7500–2600 cal BP)

Around 7500 cal BP, at the onset of the ceramic Neolithic period (Stöckli, 2016), sediments become entirely varved, production increases significantly and carbonates decrease. Erosion increases progressively, following the same trajectory as production (Fig. 5). Pollen records indicate an expansion of *Fagus sylvatica* forests after 7500 cal BP (Rey et al., 2019a; Tinner and Lotter, 2006). Concurrently, microscopic-charcoal-inferred regional forest fires and agricultural activity increase (Fig. 5), marking the onset of noticeable human activities in the catchment and the development of settlements around the lake (Harb, 2017) (Fig. 5). Cultivated plants (*Cerealia-type*), expansion of weeds i.e *Plantago lanceolata*, apophytes i.e *Urtica* and sporadic *Sporormiella* fungal spores (Rey et al., 2019a) indicate important agricultural and pastoral activities that increase N and mainly P pools in the catchment soil (Ross et al., 1999; Wang et al., 2009). Human induced forest openings increased surface runoff that favored nutrient input into the lake and increased lake production (Fig. 6d).

Meromixis is widespread and seems to result from the combined effect of high summer temperature, closed forest (TP>80%) and wind protection, and high aquatic production (Fig. 5, 6c). Ca counts decline in periods with high production and stable stratification suggesting that (i) endogenic calcite precipitation was reduced as a result of Ca^{2+} depletion in the epilimnion, and/or (ii) carbonates were dissolved in cold and low pH hypolimnetic waters (Wetzel, 2001). Calcite dissolution contributes to the higher density of the monimolimnetic waters (Boehrer et al., 2017; Schmidt et al., 2002). Interestingly, meromixis is interrupted repeatedly during phases of local deforestation, which coincide with human settlements and agriculture on the lakeshore and in the catchment (Fig. 6d). Conversely, afforestation after land abandonment restores

meromixis (Fig. 6c). More details about the processes of onset and cease of meromictic phases are discussed in Section 5.3.

5.2.4 Zone VI (2600 cal BP–present times)

During the Iron and Roman Ages, between 2600 and 1600 cal BP, sediments are mostly homogeneous with some varved segments. Aquatic production and summer temperatures decrease. Erosion increases sharply after 2000 cal BP (Fig. 5). Decreasing tree pollen indicates a further massive opening of vegetation. Bphe is completely absent in this part indicating good oxygen conditions. A further increase in cultural and pastoral pollen indicators (*Cerealia-type*, *Plantago lanceolata*, *Urtica*, *Sporormiella* fungal spores) (Rey et al., 2019a) indicates intensified land use in the catchment increasing the nutrient input into the lake with a concomitant increase in aquatic production (Fig. 6d). This has been observed also at other sites with extensive lakeside settlements in that period (Haas et al., 2019; Zolitschka et al., 2003). Archaeological findings indicate settlements around the city of Bern (8 km south of the lake), but not directly at the lake during that time.

After the onset of the Middle Ages around 1500 cal BP, primary production increases substantially. Tree pollen decreases significantly (<30%), and cultural pollen indicators increase (Fig. 5). This, combined with the extensive forest fire peaks and increased erosion indicate a re-intensification of land use, finally leading to the open landscape of today with drastic changes in terrestrial ecosystems. Holomictic conditions prevailed except for a short period with weak seasonal anoxia around 800 cal BP (Middle Ages; see Fig. S5 in supplementary material). This is most probably driven by the Medieval Warm Period and high aquatic production, which provided pronounced stratification that favored anoxygenic phototrophic bacteria proliferation (Imhoff, 2014; Vila et al., 1998). During the Little Ice Age production decreases, before it reaches the highest peak observed ever in Modern Times with 20th century eutrophication. These findings agree with several other records on the Swiss

Plateau (Lotter, 2001; Züllig, 1989), where intensive agriculture and urbanization have been recognized as major drivers of excessive nutrient inputs and accelerated deterioration of trophic states (Makri et al., 2019).

5.3 Mid-Holocene meromictic cycles and the role of early human impact

Meromixis occurred and ceased in Moossee several times during the past 15,000 years, influenced by such factors as aquatic production, forest cover, and climate (Fig. 7a-c). The high-resolution HSI-inferred Bphe and TChl records allow the interplay of these factors to be examined for individual meromictic events. Until 7500 cal BP, around the onset of the ceramic Neolithic, Moossee was mostly holomictic except for some instances of prolonged stratification with anoxic bottom waters driven mainly by warmer summers and dense forest cover. After 7500 cal BP, when the lake became more productive and the expansion of forests reduced wind exposure, meromictic events became more frequent.

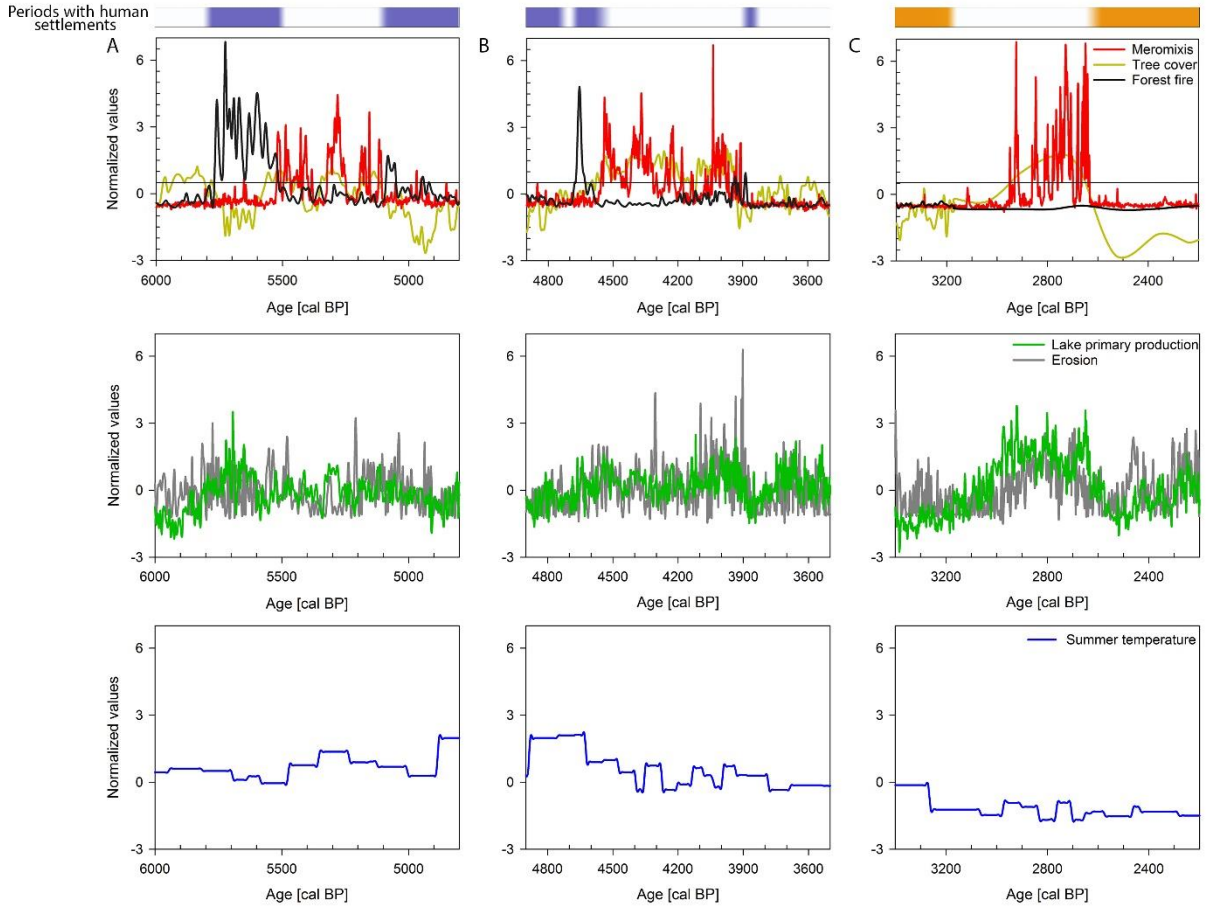

534

535 **Fig. 7:** Close-ups of the three main meromictic events (a), (b) and (c) in the Neolithic and
536 Bronze Ages in relation to the variability of tree cover (tree pollen), forest fires (microscopic
537 charcoal; Rey et al., 2019a), lake primary production (TChl), erosion (Ti), and summer
538 temperature (Heiri et al., 2015). All the data are normalized. The periods of human settlements
539 around the lake, based on archaeological findings (Harb, 2017) are shown in purple, and periods
540 with high cultural pollen (Rey et al., 2019a) are shown in orange. The black horizontal line in
541 the top panels corresponds to the 80% tree pollen that is the threshold that triggers meromixis.

542

543 Figs. 7a-c show close-ups for three meromictic events between 6000 and 2200 cal BP, with
544 the indicators for meromixis ($RABD_{845}$), forest cover (TP percentages), microscopic charcoal
545 (fire activity) (Rey et al., 2019a), aquatic production ($RABD_{673}$), erosion (Ti), and chironomid-
546 inferred summer temperatures (Heiri et al., 2015). After 7500 cal BP, prior to any human
547 intervention, forest composition changed significantly in response to a warmer and moister

548 climate, with a decrease in hazel shrubland dominance and the expansion of mixed beech forests
549 (Rey et al., 2019a, 2017), (TP>80%) (Fig. 7a). Yet production was still relatively low, and the
550 lake was mixing completely annually. From 5750 to 5600 cal BP, extended forest fires reduced
551 tree cover significantly; this coincided with the presence of local Neolithic pile dwellings
552 around the lake (Harb, 2017). Intensified agricultural activities at that time (Rey et al., 2019a)
553 and forest fires indicate intentionally disrupted forests with slash-and-burning for arable and
554 pastoral farming (Rey et al., 2019a; Tinner et al., 2005). During this phase of open landscape,
555 erosion and production increased. We interpret this as the result of increased runoff and
556 consequent nutrient enrichment of the lake water due to pastoralism and intense agricultural
557 activity around the lake (Bajard et al., 2018; Pini et al., 2017). Around 5600 cal BP, forest fires
558 started to decline, and reforestation began after land abandonment. By 5530 cal BP, TP recovers
559 and exceeds 80%, suggesting that the forest canopy closed (Braun-Blanquet, 1932; Jennings et
560 al., 2009). It was precisely at this point that meromixis appeared and persisted for the next 430
561 years (until 5100 cal BP; Fig. 7a). At 5100 cal BP, the next phase of forest fires appeared with
562 the onset of the next human lakeshore settlement (Harb, 2017). TP drops below the threshold
563 of 80%, indicating that forest opening and meromixis ceased. From 5100 to 4550 cal BP, human
564 presence around the lake persisted. High erosional input prompted higher aquatic production.
565 Under such conditions (TP<80%), the lake was mixing annually. Summer temperature did not
566 show any variation that could have affected lake mixing during this period.

567 The same cycle occurred in the second and third meromixis events (Fig. 7b, c). Repeatedly,
568 meromixis occurred exactly when TP surpassed 80% (at 4550 cal BP and at 2950 cal BP) and
569 disappeared when TP dropped below 80% (at 3900 cal BP and 2650 cal BP, respectively).
570 These meromixis events lasted for 650 and 300 years each. They occurred at a time when
571 summer temperatures decreased. Negative effects of erosion, turbidity and light conditions on
572 the presence of anoxygenic phototrophic bacteria, as observed by Parkin and Broth (1980), do
573 not seem to have played a role in Moossee (Fig. 7c).

We suggest that during the Neolithic and Bronze Ages the establishment of meromixis was strongly linked to dense forest cover (TP>80%) that reduced wind shear in the catchment and around the lake (Fig. 6c), whereas meromixis was apparently disrupted by the open landscape that resulted from anthropogenic disturbance in the catchment (Fig. 6d). Although here we show for the first time that an 80% TP threshold repeatedly determined lake mixing during the mid- and late Holocene, catchment forest dominance and the role of wind shear bringing additional kinetic energy in the lake water column has also been inferred for other lakes (Lotter, 2001; Stevens et al., 2000). In addition, the threshold of 80% TP triggering meromixis may not be applicable to all lakes depending on size, morphometry and catchment topography. The differences in lake water density in biogenic meromixis is governed by endogenic rather than allogenic import of solutes. Hence, the relationship between lake depth and surface area (relative depth) plays an important role in the establishment of biogenic meromixis (Stewart et al., 2009). Moossee has a maximum depth of 22 m and surface area of 0.31 km^2, which result in a relative depth of ca. 2.6%. Deep lakes with small surface areas (i.e. relative depth>4%) tend to exhibit greater stability and are less easily mixed by wind as those with low relative depth (Hutchinson, 1957; Wetzel and Likens, 1991). On the other hand the local catchment topography can also have an effect on prevailing winds and hence the extent of vertical mixing (Walker and Likens, 1974).

6. Conclusions

The goal of this study was to investigate long-term lake ecosystem dynamics, paleoproduction, meromixis, and their responses to catchment processes, landscape evolution and human impact since the Late Glacial in Moossee, Switzerland.

Periods of Ti-inferred soil erosion and intensive surface processes occurred between 15,000 and 14,400 cal BP and from 2000 cal BP onwards. Conversely, erosion was reduced and the landscape was stable between 14,400 and 2000 cal BP. In periods of low human impact,

15,000–7500 cal BP, trophic state development in the lake was closely linked to vegetation cover that was mostly influenced by climate. Until the onset of the Neolithic, at 7500 cal BP, the lake was mostly holomictic.

During times of intensive anthropogenic presence in the catchment and land-use changes after 7500 cal BP, higher nutrient inputs due to agricultural and pastoral activities stimulated significant aquatic primary production, with relative maxima in the late Bronze Age and Middle Ages and an unprecedented peak in the 20th Century. During the Neolithic and Bronze Ages, meromixis occurred and ceased repeatedly. Our analysis suggests the following conceptual model: provided that conditions such as elevated aquatic production and warm summer temperatures were favorable, deforestation around the lake (TP<80%) and consequent stronger wind shear ceased meromixis, whereas transient reforestation after land abandonment let meromixis re-establish as the forest closed and tree pollen rose above 80%.

We conclude that the repeated meromictic cycles after the onset of the Neolithic, regulated by land use and aquatic production, document clearly how millennial-old prehistoric human impact had already modified the biogeochemical cycle in the lake long before the unprecedented anthropogenic disturbance recorded in the 20th century. Similar additional studies will improve our understanding of human effects on freshwater ecosystems over longer time scales.

Acknowledgements

This work was supported by the Hans Sigrist Foundation and the Swiss National Science Foundation Grants (SNF 200021_172586 and SNF 200021_149203/1). SM and MG designed this study and prepared the manuscript. SM performed the analytical laboratory work and data analysis. FR provided the pollen data and radiocarbon dating. AG performed XRF scanning. All co-authors commented on the manuscript. We thank Oliver Heiri for providing the chironomid-inferred summer temperatures. Special thanks go to Flavio S. Anselmetti, Christoph Butz, and Tobias Schneider for their help and contribution to this paper. We thank the two anonymous reviewers and the Editor for the constructive and thoughtful comments.

Declarations of interest: none

Data availability

Appendix A. Supplementary data

652 **References**

653 Ammann, B., 1985. Lobsigensee - Late-Glacial and Holocene environments of a lake on the
654 Central Swiss Plateau. Introduction and palynology: vegetational history and core
655 correlation at Lobsigensee (Swiss Plateau). Diss Bot 87, 125–137.
656 Ammann, B., Leeuwen, J., van der Knaap, W., Lischke, H., Heiri, O., Tinner, W., 2013a.
657 Vegetation responses to rapid warming and to minor climatic fluctuations during the
658 Late-Glacial Interstadial (GI-1) at Gerzensee (Switzerland). Palaeogeogr. Palaeoclimatol.
659 Palaeoecol. 391, 40–59. https://doi.org/10.1016/j.palaeo.2012.07.010
660 Ammann, B., van Raden, U.J., Schwander, J., Eicher, U., Gilli, A., Bernasconi, S.M., van
661 Leeuwen, J.F.N., Lischke, H., Brooks, S.J., Heiri, O., Nováková, K., van Hardenbroek,
662 M., von Grafenstein, U., Belmecheri, S., van der Knaap, W.O., Magny, M., Eugster, W.,
663 Colombaroli, D., Nielsen, E., Tinner, W., Wright, H.E., 2013b. Responses to rapid
664 warming at Termination 1a at Gerzensee (Central Europe): Primary succession, albedo,
665 soils, lake development, and ecological interactions. Palaeogeogr. Palaeoclimatol.
666 Palaeoecol. 391, 111–131. https://doi.org/https://doi.org/10.1016/j.palaeo.2013.11.009
667 Baales, M., Jöris, O., Street, M., Bittmann, F., Weninger, B., Wiethold, J., 2002. Impact of the
668 Late Glacial Eruption of the Laacher See Volcano, Central Rhineland, Germany. Quat.
669 Res. 58, 273–288. https://doi.org/10.1006/QRES.2002.2379
670 Bajard, M., Etienne, D., Quinsac, S., Dambrine, E., Sabatier, P., Frossard, V., Gaillard, J.,
671 Develle, A.L., Poulenard, J., Arnaud, F., Dorioz, J.M., 2018. Legacy of early
672 anthropogenic effects on recent lake eutrophication (Lake Bénit, northern French Alps).
673 Anthropocene 24, 72–87. https://doi.org/10.1016/j.ancene.2018.11.005
674 Bajard, M., Poulenard, J., Sabatier, P., Develle, A.L., Giguet-Covex, C., Jacob, J., Crouzet,
675 C., David, F., Pignol, C., Arnaud, F., 2017a. Progressive and regressive soil evolution
676 phases in the Anthropocene. Catena 150, 39–52.
677 https://doi.org/10.1016/j.catena.2016.11.001

678 Bajard, M., Poulenard, J., Sabatier, P., Etienne, D., Ficetola, F., Chen, W., Gielly, L.,
679 Taberlet, P., Develle, A.L., Rey, P.J., Moulin, B., de Beaulieu, J.L., Arnaud, F., 2017b.
680 Long-term changes in alpine pedogenetic processes: Effect of millennial agro-
681 pastoralism activities (French-Italian Alps). Geoderma 306, 217–236.
682 https://doi.org/10.1016/j.geoderma.2017.07.005
683 Blant, M., Moretti, M., Tinner, W., 2010. Effect of climatic and palaeoenvironmental changes
684 on the occurrence of Holocene bats in the Swiss Alps. The Holocene 20, 711–721.
685 https://doi.org/10.1177/0959683609358912
686 Boehrer, B., von Rohden, C., Schultze, M., 2017. Physical Features of Meromictic Lakes:
687 Stratification and Circulation, in: Gulati, R.D., Zadereev, E.S., Degermendzhi, A.G.
688 (Eds.), Ecology of Meromictic Lakes. Springer International Publishing, Cham, pp. 15–
689 34. https://doi.org/10.1007/978-3-319-49143-1_2
690 Braun-Blanquet, J., 1932. Plant sociology: the study of plant communities. McGraw-Hill,
691 New York.
692 Butz, C., Grosjean, M., Fischer, D., Wunderle, S., Tylmann, W., Rein, B., 2015.
693 Hyperspectral imaging spectroscopy: a promising method for the biogeochemical
694 analysis of lake sediments. J. Appl. Remote Sens. 9, 096031.
695 https://doi.org/10.1117/1.JRS.9.096031
696 Butz, C., Grosjean, M., Goslar, T., Tylmann, W., 2017. Hyperspectral imaging of sedimentary
697 bacterial pigments: a 1700-year history of meromixis from varved Lake Jaczno,
698 northeast Poland. J. Paleolimnol. 58, 57–72. https://doi.org/10.1007/s10933-017-9955-1
699 Butz, C., Grosjean, M., Poraj-Górska, A., Enters, D., Tylmann, W., 2016. Sedimentary
700 Bacteriopheophytin a as an indicator of meromixis in varved lake sediments of Lake
701 Jaczno, north-east Poland, CE 1891–2010. Glob. Planet. Change 144, 109–118.
702 https://doi.org/10.1016/j.gloplacha.2016.07.012
703 Das, B., Vinebrooke, R.D., Sanchez-Azofeifa, A., Rivard, B., Wolfe, A.P., 2005. Inferring

sedimentary chlorophyll concentrations with reflectance spectroscopy: a novel approach to reconstructing historical changes in the trophic status of mountain lakes. Can. J. Fish. Aquat. Sci. 62, 1067–1078. https://doi.org/10.1139/f05-016

Dearing, J.A., Battarbee, R.W., Dikau, R., Larocque, I., Oldfield, F., 2006. Human--environment interactions: learning from the past. Reg. Environ. Chang. 6, 1–16. https://doi.org/10.1007/s10113-005-0011-8

Diao, M., Sinnige, R., Kalbitz, K., Huisman, J., Muyzer, G., 2017. Succession of bacterial communities in a seasonally stratified lake with an anoxic and sulfidic hypolimnion. Front. Microbiol. 8. https://doi.org/10.3389/fmicb.2017.02511

Dubois, N., Saulnier-Talbot, É., Mills, K., Gell, P., Battarbee, R., Bennion, H., Chawchai, S., Dong, X., Francus, P., Flower, R., Gomes, D.F., Gregory-Eaves, I., Humane, S., Kattel, G., Jenny, J., Langdon, P., Massaferro, J., McGowan, S., Mikomägi, A., Ngoc, N.T.M., Ratnayake, A.S., Reid, M., Rose, N., Saros, J., Schillereff, D., Tolotti, M., Valero-Garcés, B., 2018. First human impacts and responses of aquatic systems: A review of palaeolimnological records from around the world. Anthr. Rev. 5, 28–68. https://doi.org/10.1177/2053019617740365

Fiedor, J., Fiedor, L., Kammhuber, N., Scherz, A., Scheer, H., 2002. Photodynamics of the bacterlochlorophyll-carotenoid system. 2. Influence of central metal, solvent and beta-carotene on photobleaching of bacteriochlorophyll derivatives. Photochem. Photobiol. 76, 145–152. https://doi.org/https://doi.org/10.1562/0031-8655(2002)076<0145:potbcs>2.0.co;2

Friedrich, J., Janssen, F., Aleynik, D., Bange, H.W., Boltacheva, N., Çagatay, M.N., Dale, A.W., Etiope, G., Erdem, Z., Geraga, M., Gilli, A., Gomoiu, M.T., Hall, P.O.J., Hansson, D., He, Y., Holtappels, M., Kirf, M.K., Kononets, M., Konovalov, S., Lichtschlag, A., Livingstone, D.M., Marinaro, G., Mazlumyan, S., Naeher, S., North, R.P., Papatheodorou, G., Pfannkuche, O., Prien, R., Rehder, G., Schubert, C.J., Soltwedel, T.,

730 Sommer, S., Stahl, H., Stanev, E. V., Teaca, A., Tengberg, A., Waldmann, C., Wehrli,
731 B., Wenzhöfer, F., 2014. Investigating hypoxia in aquatic environments: diverse
732 approaches to addressing a complex phenomenon. Biogeosciences 11, 1215–1259.
733 https://doi.org/10.5194/bg-11-1215-2014
734 Gell, P., Fritz, S., Battarbee, R., Tibby, J., 2007. LIMPACS-Human and Climate Interactions
735 with Lake Ecosystems: setting research priorities in the study of the impact of
736 salinisation and climate change on lakes, 2005-2010. Hydrobiologia 591, 99–101.
737 https://doi.org/10.1007/s10750-007-0801-8
738 Geoportal des Kantons Bern [WWW Document], 2019. Direktion für Inn. und Justiz Amt für
739 Geoinf. URL https://www.geo.apps.be.ch/de/ (accessed 12.22.19).
740 Guthruf, J., Guthruf-Seiler, K., Zeh, M., 1999. Petits plans d'eau du canton de Berne. Bern.
741 Guthruf, K., Maurer, V., Rico, R., Zeh, M., Zweifel, N., 2015. Zustand der Kleinseen 2013.
742 Bern.
743 Haas, M., Baumann, F., Castella, D., Haghipour, N., Reusch, A., Strasser, M., Eglinton, T.I.,
744 Dubois, N., 2019. Roman-driven cultural eutrophication of Lake Murten, Switzerland.
745 Earth Planet. Sci. Lett. 505, 110–117. https://doi.org/10.1016/J.EPSL.2018.10.027
746 Hakala, A., 2004. Meromixis as a part of lake evolution - Observations and a revised
747 classification of true meromictic lakes in Finland. Boreal Environ. Res. 9, 37–53.
748 Hall, K.J., Northcote, T.G., 2012. Meromictic Lakes, in: Bengtsson, L., Herschy, R.W.,
749 Fairbridge, R.W. (Eds.), Encyclopedia of Lakes and Reservoirs. Springer Netherlands,
750 Dordrecht, pp. 519–524. https://doi.org/10.1007/978-1-4020-4410-6_127
751 Harb, C., 2017. Moosseedorf, Moossee Ein Überblick über 160 Jahre Pfahlbauforschung.
752 Heiri, O., Ilyashuk, B., Millet, L., Samartin, S., Lotter, A.F., 2015. Stacking of discontinuous
753 regional palaeoclimate records: Chironomid-based summer temperatures from the Alpine
754 region. The Holocene 25, 137–149. https://doi.org/10.1177/0959683614556382
755 Hongve, D., 1997. Cycling of iron, manganese, and phosphate in a meromictic lake. Limnol.

Oceanogr. 42, 635–647. https://doi.org/10.4319/lo.1997.42.4.0635

Hutchinson, G.E., 1957. A Treatise on Limnology, Geography, Physics and Chemistry. John Wiley and Sons, New York. https://doi.org/https://doi.org/10.1017/S0016756800062634

Imboden, D M, Wüest, A., 1995. Mixing Mechanisms in Lakes, in: Lerman, A., Imboden, Dieter M, Gat, J.R. (Eds.), Physics and Chemistry of Lakes. Springer Berlin Heidelberg, Berlin, Heidelberg, pp. 83–138. https://doi.org/10.1007/978-3-642-85132-2_4

Imhoff, J.F., 2014. The Family Chromatiaceae, in: Rosenberg, E., DeLong, E.F., Lory, S., Stackebrandt, E., Thompson, F. (Eds.), The Prokaryotes: Gammaproteobacteria. Springer Berlin Heidelberg, Berlin, Heidelberg, pp. 151–178. https://doi.org/10.1007/978-3-642-38922-1_295

Jeffrey, S.W., Humphrey, G.F., 1975. New spectrophotometric equations for determining chlorophylls a, b, c1 and c2 in higher plants, algae and natural phytoplankton. Biochem. und Physiol. der Pflanz. 167, 191–194. https://doi.org/10.1016/S0015-3796(17)30778-3

Jennings, M.D., Faber-Langendoen, D., Loucks, O.L., Peet, R.K., Roberts, D., 2009. Standards for associations and alliances of the U.S. National Vegetation Classification. Ecol. Monogr. 79, 173–199. https://doi.org/10.1890/07-1804.1

Jenny, H., 1980. The Soil Resource Origin and Behavior. Springer-Verlag, New York, NY. https://doi.org/10.1007/978-1-4612-6112-4

Jenny, J.-P., Arnaud, F., Dorioz, J.-M., Covex, C.G., Frossard, V., Sabatier, P., Millet, L., Reyss, J.-L., Tachikawa, K., Bard, E., Pignol, C., Soufi, F., Romeyer, O., Perga, M.-E., 2013. A spatiotemporal investigation of varved sediments highlights the dynamics of hypolimnetic hypoxia in a large hard-water lake over the last 150 years. Limnol. Oceanogr. 58, 1395–1408. https://doi.org/10.4319/lo.2013.58.4.1395

Jenny, J.-P., Normandeau, A., Francus, P., Taranu, Z.E., Gregory-Eaves, I., Lapointe, F., Jautzy, J., Ojala, A.E.K., Dorioz, J.-M., Schimmelmann, A., Zolitschka, B., 2016. Urban point sources of nutrients were the leading cause for the historical spread of hypoxia

across European lakes. Proc. Natl. Acad. Sci. 113, 12655–12660. https://doi.org/https://doi.org/10.1073/pnas.1605480113

Jewell, P.L., Käuferle, D., Güsewell, S., Berry, N.R., Kreuzer, M., Edwards, P.J., 2007. Redistribution of phosphorus by cattle on a traditional mountain pasture in the Alps. Agric. Ecosyst. Environ. 122, 377–386. https://doi.org/10.1016/j.agee.2007.02.012

Koinig, K.A., Shotyk, W., Lotter, A.F., Ohlendorf, C., Sturm, M., 2003. 9000 years of geochemical evolution of lithogenic major and trace elements in the sediment of an alpine lake - the role of climate, vegetation, and land-use history. J. Paleolimnol. 30, 307–320.

Lang, G., 1994. Quartäre Vegetationsgeschichte Europas : Methoden und Ergebnisse. Jena: G. Fischer, New York.

Leavitt, P.R., Hodgson, D., 2001. Sedimentary Pigments, in: Smol, J., Birks, H., Last, W. (Eds.), Tracking Environmental Change Using Lake Sediments. Kluwer, Dordrecht, pp. 295–325. https://doi.org/10.1007/0-306-47668-1_15

Löffler, H., 1987. An early meromictic stage in Lobsigensee (Switzerland) as evidenced by ostracods and Chaoborus, in: Löffler, H. (Ed.), Paleolimnology IV. Springer Netherlands, Dordrecht, pp. 309–314.

Lotter, A.F., 2001. The palaeolimnology of Soppensee (Central Switzerland), as evidenced by diatom, pollen, and fossil-pigment analyses. J. Paleolimnol. 25, 65–79. https://doi.org/10.1023/A:1008140122230

Lotter, A.F., Heiri, O., Brooks, S., van Leeuwen, J.F.N., Eicher, U., Ammann, B., 2012. Rapid summer temperature changes during Termination 1a: high-resolution multi-proxy climate reconstructions from Gerzensee (Switzerland). Quat. Sci. Rev. 36, 103–113. https://doi.org/10.1016/J.QUASCIREV.2010.06.022

Mailänder, R., Veit, H., 2001. Periglacial cover-beds on the Swiss Plateau: indicators of soil, climate and landscape evolution during the Late Quaternary. CATENA 45, 251–272.

https://doi.org/10.1016/S0341-8162(01)00151-5

Makri, S., Lami, A., Lods-Crozet, B., Loizeau, J.-L., 2019. Reconstruction of trophic state shifts over the past 90 years in a eutrophicated lake in western Switzerland, inferred from the sedimentary record of photosynthetic pigments. J. Paleolimnol. 61. https://doi.org/10.1007/s10933-018-0049-5

MeteoSwiss, 2019. Evolution annuelle température/ensoleillement précipitations. Zurich-Airport.

Meyer, K.M., Macalady, J.L., Fulton, J.M., Kump, L.R., Schaperdoth, I., Freeman, K.H., 2011. Carotenoid biomarkers as an imperfect reflection of the anoxygenic phototrophic community in meromictic Fayetteville Green Lake. Geobiology 9, 321–329. https://doi.org/10.1111/j.1472-4669.2011.00285.x

Murtagh, F., Legendre, P., 2014. Ward's Hierarchical Agglomerative Clustering Method: Which Algorithms Implement Ward's Criterion? J. Classif. 31, 274–295. https://doi.org/10.1007/s00357-014-9161-z

Naeher, S., Gilli, A., North, R.P., Hamann, Y., Schubert, C.J., 2013. Tracing bottom water oxygenation with sedimentary Mn/Fe ratios in Lake Zurich, Switzerland. Chem. Geol. 352, 125–133. https://doi.org/10.1016/J.CHEMGEO.2013.06.006

Naeher, S., Smittenberg, R.H., Gilli, A., Kirilova, E.P., Lotter, A.F., Schubert, C.J., 2012. Impact of recent lake eutrophication on microbial community changes as revealed by high resolution lipid biomarkers in Rotsee (Switzerland). Org. Geochem. 49, 86–95. https://doi.org/10.1016/j.orggeochem.2012.05.014

Niessen, F., Kelts, K., 1989. The deglaciation and Holocene sedimentary evolution of southern perialpine Lake Lugano - implications for Alpine paleoclimate. Eclogae Geol. Helv. 82, 235–263.

Parkin, T.B., Brock, T.D., 1980. Photosynthetic bacterial production in lakes: The effects of light intensity. Limnol. Oceanogr. 25, 711–718.

834 https://doi.org/10.4319/lo.1980.25.4.0711
835 Pini, R., Ravazzi, C., Raiteri, L., Guerreschi, A., Castellano, L., Comolli, R., 2017. From
836 pristine forests to high-altitude pastures: an ecological approach to prehistoric human
837 impact on vegetation and landscapes in the western Italian Alps. J. Ecol. 105, 1580–
838 1597. https://doi.org/10.1111/1365-2745.12767
839 R Core Team, 2015. R: A language and environment for statistical computing.
840 Rach, O., Brauer, A., Wilkes, H., Sachse, D., 2014. Delayed hydrological response to
841 Greenland cooling at the onset of the Younger Dryas in western Europe. Nat. Geosci. 7,
842 109.
843 Rey, F., Gobet, E., Schwörer, C., Hafner, A., Tinner, W., 2019a. Climate impacts on
844 deglaciation and vegetation dynamics since the Last Glacial Maximum at Moossee
845 (Switzerland). Clim. Past Discuss. 2019, 1–32. https://doi.org/10.5194/cp-2019-121
846 Rey, F., Gobet, E., Schwörer, C., Wey, O., Hafner, A., Tinner, W., 2019b. Causes and
847 mechanisms of synchronous succession trajectories in primeval Central European mixed
848 Fagus sylvatica forests. J. Ecol. 107, 1392–1408. https://doi.org/10.1111/1365-
849 2745.13121
850 Rey, F., Gobet, E., Szidat, S., Lotter, A.F., Gilli, A., Hafner, A., Tinner, W., 2019c.
851 Radiocarbon wiggle matching on laminated sediments delivers high-precision
852 chronologies. Radiocarbon 61, 265–285. https://doi.org/10.1017/RDC.2018.47
853 Rey, F., Gobet, E., van Leeuwen, J.F.N., Gilli, A., van Raden, U.J., Hafner, A., Wey, O.,
854 Rhiner, J., Schmocker, D., Zünd, J., Tinner, W., 2017. Vegetational and agricultural
855 dynamics at Burgäschisee (Swiss Plateau) recorded for 18,700 years by multi-proxy
856 evidence from partly varved sediments. Veg. Hist. Archaeobot. 26, 571–586.
857 https://doi.org/10.1007/s00334-017-0635-x
858 Ross, D.J., Tate, K.R., Scott, N.A., Feltham, C.W., 1999. Land-use change: Effects on soil
859 carbon, nitrogen and phosphorus pools and fluxes in three adjacent ecosystems. Soil

Biol. Biochem. 31, 803–813. https://doi.org/10.1016/S0038-0717(98)00180-1

Samartin, S., Heiri, O., Lotter, A., Tinner, W., 2012. Climate warming and vegetation response after Heinrich event 1 (16 700-16 000 cal yr BP) in Europe south of the Alps. Clim. Past 8, 1913–1927. https://doi.org/10.5194/cp-8-1913-2012

Schmid, S.M., Fügenschuh, B., Kissling, E., Schuster, R., 2004. Tectonic map and overall architecture of the Alpine orogen. Eclogae Geol. Helv. 97, 93–117. https://doi.org/10.1007/s00015-004-1113-x

Schmidt, R., Psenner, R., Müller, J., Indinger, P., Kamenik, C., 2002. Impact of late glacial climate variations on stratification and trophic state of the meromictic lake Längsee (Austria): Validation of a conceptual model by multi proxy studies. J. Limnol. 61. https://doi.org/10.4081/jlimnol.2002.49

Schneider, T., Rimer, D., Butz, C., Grosjean, M., 2018. A high-resolution pigment and productivity record from the varved Ponte Tresa basin (Lake Lugano, Switzerland) since 1919: insight from an approach that combines hyperspectral imaging and high-performance liquid chromatography. J. Paleolimnol. 60, 381–398. https://doi.org/10.1007/s10933-018-0028-x

Schwalb, A., Hadorn, P., Thew, N., Straub, F., 1998. Evidence for Late Glacial and Holocene environmental changes from subfossil assemblages in sediments of Lake Neuchâtel, Switzerland. Palaeogeogr. Palaeoclimatol. Palaeoecol. 140, 307–323. https://doi.org/10.1016/S0031-0182(98)00025-X

Smith, V.H., Schindler, D.W., 2009. Eutrophication science: where do we go from here? Trends Ecol. Evol. 24, 201–207. https://doi.org/https://doi.org/10.1016/j.tree.2008.11.009

Stevens, L., Ito, E., Olson, D., 2000. Relationship of Mn-carbonates in varved lake-sediments to catchment vegetation in Big Watab Lake, MN, USA. J. Paleolimnol. 24, 199–211. https://doi.org/10.1023/A:1008169526577

886 Stewart, K.M., Walker, K.F., Likens, G.E., 2009. Meromictic Lakes. Encycl. Inl. Waters 589–
887 602. https://doi.org/10.1016/B978-012370626-3.00027-2
888 Stöckli, W.E., 2016. Urgeschichte der Schweiz im Überblick (15000 v.Chr.-Christi Geburt):
889 die Konstruktion einer Urgeschichte, Antiqua: Verl. Schweizerische Gesellschaft für Ur-
890 und Frühgeschichte. Archäologie Schweiz.
891 Tinner, W., Conedera, M., Ammann, B., Lotter, A.F., 2005. Fire ecology north and south of
892 the Alps since the last ice age. The Holocene 15, 1214–1226.
893 https://doi.org/10.1191/0959683605hl892rp
894 Tinner, W., Lotter, A.F., 2006. Holocene expansions of *Fagus silvatica* and *Abies alba* in
895 Central Europe: where are we after eight decades of debate? Quat. Sci. Rev. 25, 526–
896 549. https://doi.org/10.1016/J.QUASCIREV.2005.03.017
897 Tonolla, M., Peduzzi, R., Hahn, D., 2005. Long-term population dynamics of phototrophic
898 sulfur bacteria in the chemocline of Lake Cadagno, Switzerland. Appl. Environ.
899 Microbiol. 71, 3544–3550. https://doi.org/10.1128/AEM.71.7.3544-3550.2005
900 Tonolla, M., Peduzzi, S., Hahn, D., Peduzzi, R., 2003. Spatio-temporal distribution of
901 phototrophic sulfur bacteria in the chemocline of meromictic Lake Cadagno
902 (Switzerland). FEMS Microbiol. Ecol. 43, 89–98. https://doi.org/10.1016/S0168-
903 6496(02)00354-9
904 Veit, H., Trauerstein, M., Preusser, F., Messmer, T., Gnägi, C., Zech, R., Wüthrich, L., 2017.
905 Late Glacial/Early Holocene slope deposits on the Swiss Plateau: Genesis and palaeo-
906 environment. CATENA 158, 102–112. https://doi.org/10.1016/J.CATENA.2017.06.012
907 Vila, X., Abella, C.A., Figueras, J.B., Hurley, J.P., 1998. Vertical models of phototrophic
908 bacterial distribution in the metalimnetic microbial communities of several freshwater
909 North-American kettle lakes. FEMS Microbiol. Ecol. 25, 287–299.
910 https://doi.org/10.1016/S0168-6496(98)00010-5
911 Walker, K., Likens, G., 1974. Meromixis and a reconsidered typology of lake circulation

912 patterns. Verhandlungen der Int. Vereinigung für Theor. und Angew. Limnol. 19, 422–
913 458. https://doi.org/10.1080/03680770.1974.11896084
914 Wang, Y., Zhang, X., Huang, C., 2009. Spatial variability of soil total nitrogen and soil total
915 phosphorus under different land uses in a small watershed on the Loess Plateau, China.
916 Geoderma 150, 141–149. https://doi.org/10.1016/j.geoderma.2009.01.021
917 Wetzel, R.G., 2001. Limnology: Lake and River Ecosystems, 3rd ed, Journal of Phycology.
918 Acedemic Press.
919 Wetzel, R.G., Likens, G.E., 1991. Limnological Analyses, 2nd ed. Springer-Verlag, New
920 York. https://doi.org/https://doi.org/10.1002/rrr.3450070410
921 Wirth, S.B., Gilli, A., Niemann, H., Dahl, T.W., Ravasi, D., Sax, N., Hamann, Y., Peduzzi,
922 R., Peduzzi, S., Tonolla, M., Lehmann, M.F., Anselmetti, F.S., 2013. Combining
923 sedimentological, trace metal (Mn, Mo) and molecular evidence for reconstructing past
924 water-column redox conditions: The example of meromictic Lake Cadagno (Swiss Alps).
925 Geochim. Cosmochim. Acta 120, 220–238. https://doi.org/10.1016/j.gca.2013.06.017
926 Woolway, R.I., Merchant, C.J., 2019. Worldwide alteration of lake mixing regimes in
927 response to climate change. Nat. Geosci. 12, 271–276. https://doi.org/10.1038/s41561-
928 019-0322-x
929 Yurkov, V. V, Beatty, J.T., 1998. Aerobic Anoxygenic Phototrophic Bacteria. Microbiol.
930 Mol. Biol. Rev. 62, 695 LP – 724.
931 Żarczyński, M., Wacnik, A., Tylmann, W., 2019. Tracing lake mixing and oxygenation
932 regime using the Fe/Mn ratio in varved sediments: 2000 year-long record of human-
933 induced changes from Lake Żabińskie (NE Poland). Sci. Total Environ. 657, 585–596.
934 https://doi.org/10.1016/J.SCITOTENV.2018.12.078
935 Zolitschka, B., Behre, K.-E., Schneider, J., 2003. Human and climatic impact on the
936 environment as derived from colluvial, fluvial and lacustrine archives—examples from
937 the Bronze Age to the Migration period, Germany. Quat. Sci. Rev. 22, 81–100.

https://doi.org/10.1016/S0277-3791(02)00182-8

Züllig, H., 1989. Role of carotenoids in lake sediments for reconstructing trophic history during the late Quaternary. J. Paleolimnol. 2, 23–40. https://doi.org/10.1007/BF00156982